Available online at www.eccomasproceedia.org
Eccomas Proceedia COMPDYN (2023) 3936-3947

ECCOMAS
Proceedia

COMPDYN 2023
9th ECCOMAS Thematic Conference on
Computational Methods in Structural Dynamics and Earthquake Engineering
M. Papadrakakis, M. Fragiadakis (eds.)
Athens, Greece, 12-14 June 2023

# MODELING OF FRAMES WITH HYBRIDFEM, A PSEUDO-DISCRETE-FINITE MODEL INCLUDING NONLINEAR GEOMETRIC EFFECTS AND NONLINEAR MATERIALS

**Igor Bouckaert[1*], Michele Godio[2], João Pacheco de Almeida[1]**

[1]Institute of Mechanics, Materials and Civil Engineering, UCLouvain
Louvain-la-Neuve, Belgium
e-mail: {igor.bouckaert,joao.almeida}@uclouvain.be

[2] RISE Research Institutes of Sweden
Brinellgatan 4, 504 62 Boras, Sweden
e-mail: michele.godio@ri.se

**Abstract.** *In this paper, a novel numerical method for strucural analysis, called the Hybrid Discrete-Finite Element Method (HybriDFEM), is presented. In this method, a structure is modeled as an assembly of rigid blocks in contact. All the deformation is concentrated at the interfaces, which are modeled as series of distributed nonlinear multidirectional springs. The method shares similarities with the Discrete Element Methods (DEM) in its ability to account for contact interfaces and/or block deformability, and with the Applied Element Method (AEM) in the representation of interfaces as a series of normal and shear springs. However, it is close to the FEM in the way it is formulated, which offers the possibility to readily link both methods for potential hybrid applications. This paper focuses on the modeling of continuous and discontinuous frames with the HybriDFEM. It is shown how the model can do so with a nonlinear material model, and considering (or not) nonlinear geometric effects through large nodal displacements. Different nonlinear solution procedures implemented in HybriDFEM are demonstrated, such as load-control and various displacement-controlled methods. This model is able to simulmate contacts between rigid or deformable units, an important feature when it comes to the modeling of, e.g., unreinforced masonry structures, with a reasonable computational cost and a formulation that is cast within the framework of the classical FEM.*

**Keywords:** Hybrid modelling, Discrete Element Methods, Applied Element Method, $P-\Delta$ effects, masonry, frames, piers, spandrels

ISSN:2623-3347 
Peer-review under responsibility of the organizing committee of COMPDYN 2023.
doi: 10.7712/120123.10692.20680

# 1 INTRODUCTION

In structural mechanics, accurately modeling interfaces is crucial when analyzing structures that present discontinuities, either for masonry (URM) structures that are discontinuous by nature, for cracked reinforced concrete (RC) members or for soil-structure interactions. The Finite Element Method (FEM) [5, 14], which is the most widely-used modeling technique amongst practitioners, is commonly used to model structures as a continuous medium. When discontinuities arise, FEM-based modeling techniques can use homogenization techniques to average the discontinuous behaviour over the element, or use micro-modeling approaches to account explicitly for discontinuous behavior [13, 11]. The former comes with an increased computational efficacy but at the price of a loss of precision in the results and representation of the physical response, whereas the latter requires a lot of computational power.

The Discrete Element Method (DEM) [4, 9, 1] is a family of modeling techniques that can represent more accurately the discontinuous nature of material assemblies but requires more computational resources. It models a structure as an assembly of rigid elements connected through deformable contact interfaces. All DEM formulations share the characteristic that a numerical time-stepping algorithm is required, resulting in a drastically higher computational time, and the incapacity to handle static or buckling problems. Other methods treat the problem as an assembly of rigid units interconnected by deformable interfaces modeled as distributed nonlinear multidirectional springs, making it suitable for analyzing large structures in static or dynamic problems. Various formulations, such as the Rigid Block model (RB) [12], the Rigid-Body-Spring Model (RBSM) [3], the Applied Element Method (AEM) [10] and the Fiber Contact Element Method (FCEM) [7, 6], are proposed to model discontinuities with this approach. These methods are interesting because they model the structure with a limited number of degrees of freedom (DoFs) considered at the structural level [15]. This paper introduces a new method called the Hybrid Discrete-Finite Element Method (HybriDFEM), which is capable of handling discontinuities in structures. This method extends the existing FCEM method by incorporating nonlinear geometric and material models. The HybriDFEM involves a collection of rigid rectangular blocks (how block deformability can be taken into account will be explained after) interacting with each other through interfaces composed of distributed nonlinear springs, similarly to the AEM. In Section 2, some theoretical developments of the method will be covered. Then, a first benchmark problem will be introduced in Section 3, showing the ability of the HybriDFEM to model the behaviour of a continuous frame, including $P-\Delta$ effects. The results of this benchmark problem will be compared against classical FEM formulations. In Section 4, a simple masonry portal frame composed of multiple discontinuous, rigid blocks, will be simulated. The failure mechanism and the collapse load multiplier of the frame will be compared against analytical solutions from limit analysis.

# 2 THEORETICAL DEVELOPMENTS

## 2.1 Block discretisation

In the HybriDFEM method, a planar structure is modeled as a series of rigid blocks in contact through contact faces (CFs). The discretisation of the structure in $n_b$ blocks defines the total number of DoFs considered at the global level. The motion of a block is described by three kinematic variables, two translations and one rotation, which are stored in the vector of nodal displacements $\mathbf{U}$. The kinematic variables of a generic block $i$ are the displacements $U_{3i-2}$, $U_{3i-1}$ and $U_{3i}$, expressed in the global reference system $(X, Y)$. The block discretisation of a beam is shown in Figure 1.

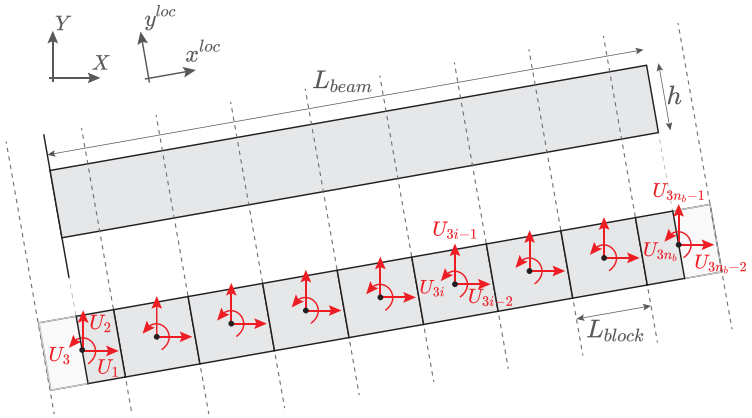


Figure 1: Block discretisation and kinematic variables of a beam at the structural level [2].

## 2.2 Contact pair discretisation

Each CF is further subdivided into a series of $n_c$ contact pairs (CPs) evenly distributed along the interface between two blocks (Figure 2b). One CP consists of three points $A$, $B$ and $C$. The two first are respectively fixed to the edge of the first and second block. A nonlinear spring is attached to point $A$ and connected to another nonlinear spring attached to point $B$ through a hinged contact point $C$ (Figure 2c). The kinematics of the contact pair is described by eight DoFs in total. The three first refer to the displacement of point $A$ and its spring's orientation, which follows the orientation of the block to which it is attached. Similarly, the three next DoFs of the CP refer to the displacement of point $B$ and its spring's orientation. The last two DoFs refer to the displacement of point C and will be condensed for the computations at the structural level.

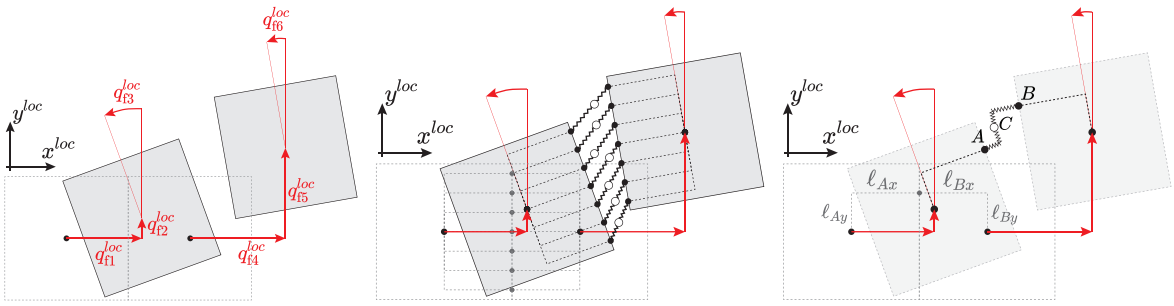


(a) (b) (c)

Figure 2: (a) Block kinematics in the local reference system (b) contact pair discretisation of the contact face (c) Isolated contact pair [2].

The kinematics of the six first DoFs of the CP can be derived solely through compatibility relations, since the position of $A$ and $B$ with respect to their respective blocks does not change, and the blocks are rigid. These first six DoFs of each CP can be directly related with the six DoFs of the adjacent blocks, $q_1^{loc}$ to $q_6^{loc}$, represented in Figure 2a. To derive the position of point $C$ (i.e., the last two DoFs of each CP), however, the relative elongations of the two pairs

of springs need to be known. They can be derived through a set of two linear equations relative to compatibility and two possibly nonlinear equations relative to equilibrium. The former states that the total CP deformation must be equal to the sum of elongation of the first and second spring, both in the normal and tangential directions (Figure 3a). By isolating the deformation of the CP without considering its rigid-body motion, nonlinear geometry is accounted for. The equations relative to equilibrium state that the forces through spring $A$ must be equal to the forces through spring $B$ (Figure 3b). These forces depend on the constitutive relations assigned to the springs, relating the spring elongation with the spring forces. The constitutive relations can represent either the behaviour at the contact between the two blocks (e.g. when modeling assemblies of rigid blocks) or can be scaled to represent the behaviour of a continuous material, where the deformation of the block is concentrated at each CF. By assigning a nonlinear constitutive relation to the springs, nonlinear material effects can be included.

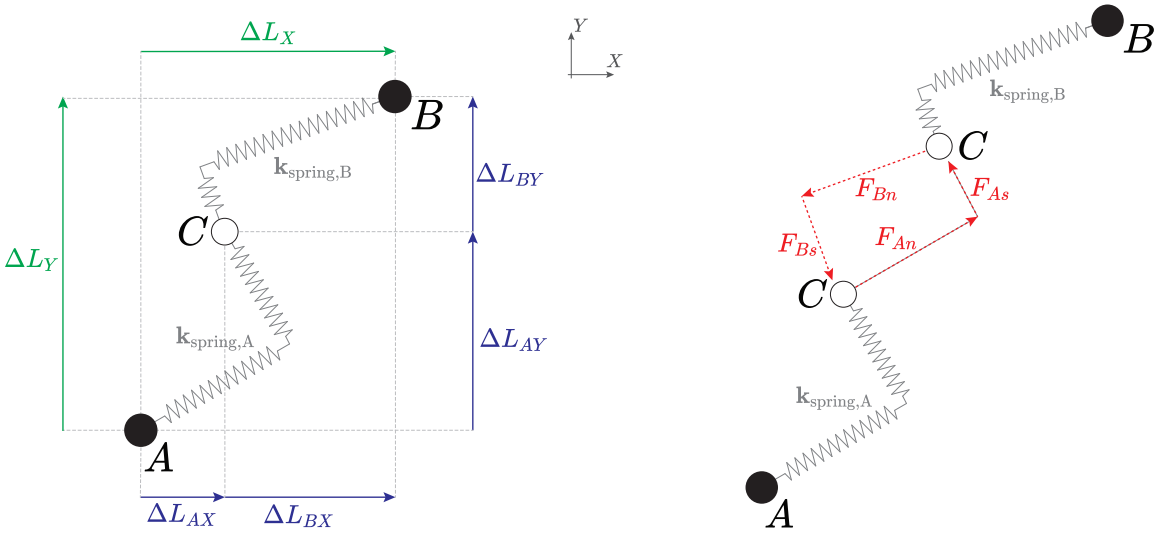


Figure 3: (a) Compatibility relation of the CP and (b) equilibrium of spring forces used to determine the position of point $C$, the relative spring elongations, and the spring forces [2].

The set of nonlinear equations relative to compatibility and equilibrium is solved by means of a Newton-Raphson solution procedure, at the end of which the forces through the springs attached to $A$ and $B$ are known, along with their relative elongations and the displacement of point $C$. This nonlinear solution procedure is referred to as the internal solution procedure, as opposed to the external solution procedure at the global level, common to the nonlinear FEM, which will be described in section 2.3.

From the spring forces, the resisting forces of each CP can be derived by equilibrium in the deformed configuration, which allows to account for nonlinear geometric effects. Finally, the resisting forces of each CF can be computed by assembling the resisting forces of all of its CPs, and the resisting forces $\mathbf{P}_r$ of the structure can be computed by assembly of the resisting forces of all CFs.

### 2.3 Solution procedure at the structural level

The steps described hereabove can be used to derive the resisting forces $\mathbf{P}_r$ of the structure associated to a given set of nodal displacements $\mathbf{U}$. From the constitutive relation assigned to the springs, an incremental relation between the spring forces and spring elongations can be derived, which corresponds to the tangent stiffness matrix of the springs. The tangent stiffness matrices of the two springs composing one CP can be used to assemble the tangent stiffness matrix of the CP, which can then be assembled into the tangent stiffness matrix of the contact face. Finally, the tangent stiffness matrix of the structure can be assembled from the stiffness matrices of all the CFs. In the case of linear elastic structures, this stiffness matrix can be used to relate directly the nodal displacements stored in $\mathbf{U}$ to the global resisting forces $\mathbf{P}_r$, and equilibrium with a given set of applied forces $\mathbf{P}$ can be found by inverting such tangent stiffness matrix (or, computationally, any solution method for linear equations). When nonlinear effects are considered, however, the nodal displacements equilibrating the resisting forces with the applied forces cannot be computed by matrix inversion, and an incremental solution procedure is required. Such incremental-iterative solution procedure, which can be for instance a Newton-Raphson (load-control), displacement-control, or work-control procedure [5], computes the tangent stiffness matrix of the structure at each iteration to achieve quadratic convergence. This solution procedure, as well as a detailed account of all the equations expressing the operations described in this Section 2, can be found elsewhere [2].

## 3 MODELING OF A CONTINUOUS FRAME WITH $P-\Delta$ EFFECTS

In this benchmark, the capacity of the HybriDFEM to approximate the behaviour of continuous structures despite its discontinuous nature, is demonstrated. This example also shows how it can capture nonlinear material and geometric effects, and how it can be coupled with classical finite elements to increase its computational efficacy.

this example consists of a one-storey one-bay $3$ m$\times 3$ m frame, in which the flexural stiffness of the columns equals twice the flexural stiffness of the beam, which is assumed to have a square cross-section of $h \times b = 0.2$ m$\times 0.2$ m. The two columns are simply supported. The material law assigned to both the column and the beam is an elastic-perfectly plastic law of the type

$$\begin{cases} \sigma = \varepsilon E_0 & \text{when} \quad \mid \varepsilon \mid \leq \varepsilon_y \\ \sigma = f_y & \text{when} \quad \mid \varepsilon \mid > \varepsilon_y \\ \tau = \gamma G_0 \end{cases}, \tag{1}$$

where $E_0 = 30$ GPa, $G_0 = 15$ GPa and $f_y = 20$ MPa.

The response of the frame is evaluated with three different models:

(a) A simple FEM model built with three Timoshenko beam elements (Figure 4a) for which nonlinear geometric effects can be included, but restricted to linear elastic response;

(b) A coupled FEM-HybriDFEM model where the columns are modeled with one such Timoshenko beam element each and the beam is modeled with one HybriDFEM element, with 40 blocks and 30 CPs per block (Figure 4b);

(c) A full HybriDFEM model where both the columns and the beams are modeled with 40 blocks and 30 contact pairs at each interface (Figure 4c).

At its current state of development, the HybriDFEM code can only handle beam-like members (one-directional members), which can be connected through rigid-node connections. Therefore, the beam and the columns are each modeled as three distinct beam-like members, and the centroid of their extremity blocks are connected through a rigid-node connection.

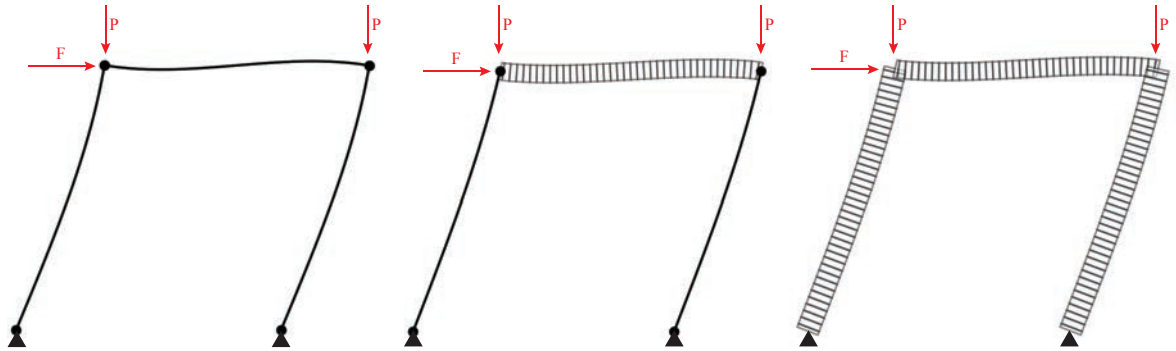


(a) (b) (c)

Figure 4: (a) full FEM model (b) coupled HybridFEM (beam)- FEM (columns) model (c) full HybriDFEM model at a horizontal displacement of 5 cm. The deformations are magnified by a factor of 20.

The lateral capacity of the frame is evaluated by applying a horizontal force $F$ at the centroid of the block located at the top left corner. The value of the applied force is controlled by means of a displacement-control monitoring the horizontal displacement $\Delta$ of the top left corner, with increments of $1$ mm up to $65$ mm. The additional weight of possible upper storeys is represented by two constant vertical downward forces of $P = 100$ kN applied at the top left and top right corners of the frame.

At first, the pushover curves of the three models are computed neglecting $P - \Delta$ effects, i.e. assuming linear geometry. For an Euler-Bernoulli beam, the horizontal force at which the material will start yielding, $F_y = 17.8$ kN can be derived analytically. Using the beam plastic moment, it is also possible to derive the maximal capacity of the frame, $F_{max} = 26.7$ kN (Figure 5a). The response of the frame in the linear range is compared with the linear FEM model, and the pushover curve of the full HybriDFEM model can be compared with the coupled FEM-HybriDFEM model, under the observation that with the HybriDFEM plastification occurs in the beam and not in the columns.

The deformed shapes of the three models at the end of the simulation, magnified by a factor of 20, are visible in Figure 4. The force-displacement response associated to the three models is visible in Figure 5a. The curves of the coupled and the full HybriDFEM model plateau at $27.3$ kN, which corresponds to a $2.3\%$ increase in maximal capacity with respect to the analytical value. The first yielded CP appears at a displacement of $21$ mm, at which the applied force equals $18.43$ kN, corresponding to a $3.5\%$ relative error with respect to the analytical value. The stresses in the beam and its deformed shape at a displacement of $\Delta = 50$ mm (Figure 6) highlight the formation of the plastic hinges at the extremities of the beam. No yielding was observed in the columns with the full HybriDFEM model, as expected. The three models show excellent agreement in the linear range. Beyond yielding, the linear FEM model can evidently not be compared with the two others. However, the pushover curve obtained with the coupled model matches very well the curve obtained with the full HybriDFEM model, since the columns

continue to behave elastically throughout the entire response. The computational time necessary to run the coupled model is 3.5 times less than that required to run the full HybriDFEM model, which illustrates one of the computational advantages of the present proposal.

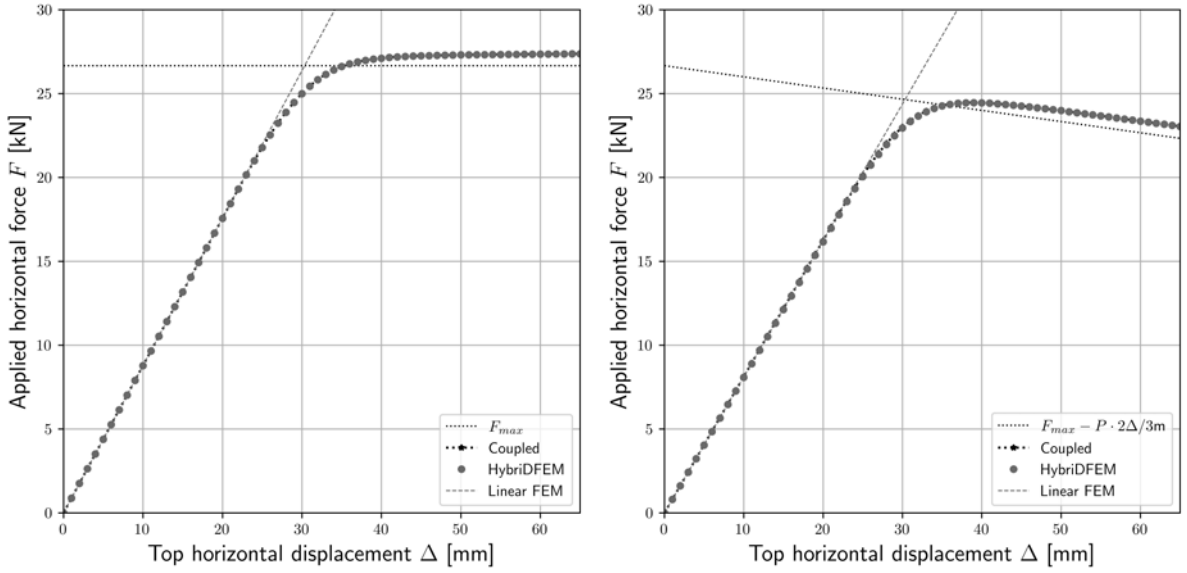


(a) (b)

Figure 5: Force-displacement curves of the frame (a) neglecting $P - \Delta$ effects, and (b) considering $P - \Delta$ effects .

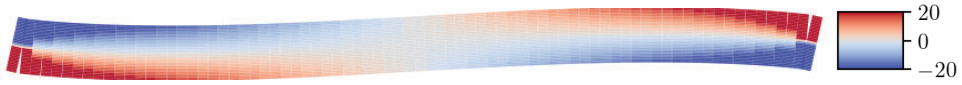


Figure 6: Stresses in the beam, in MPa, highlighting the presence of plastic hinges at the extremities of the beam.

The same three models are run considering nonlinear geometric effects. In that case, the descending branch of the pushover curve, after the plastic hinges have formed, can be derived analytically and corresponds to a horizontal line of equation $F = F_{max} - P \cdot 2\Delta/3$ m in the $F - \Delta$-plane. The responses of the three models in the linear material range, before the material yields, once again compare very well. As expected, the slope of the ascending branch is slightly lower than when nonlinear geometric effects were neglected due to the $P - \Delta$ effects. After the peak, when the plastic hinges have formed, the pushover curves of the coupled and full HybriDFEM model descend along a line parallel to the analytical one, with an error comparable to the linear case, displaying a slightly higher capacity than the analytical value. Again, the two pushover curves of the coupled and HybriDFEM model show negligible difference.

This benchmark highlights the capacity of the HybriDFEM to capture nonlinear geometric effects, with accurate simulation of the $P - \Delta$ effects in the frame, and nonlinear material effects with the appearance of plastic hinges in the beam modeled with the HybriDFEM. It also highlights the possibility to straightforwardly couple the HybriDFEM with classical FEM

formulations in zones of the structure that remain linear-elastic, making the simulation computationally more efficient. Finally, it shows that the HybriDFEM can model accurately frames made of a continuous material, despite the discontinuous nature of its formulation.

## 4 MASONRY FRAMES

This benchmark is taken from Giordano et al. [8], in which analytical formulae to determine the collapse load multiplier of a heavy masonry frame are derived through kinematic analysis. The collapse load multiplier $\alpha$ is defined as the ratio between $F_{max}$ and $W_{tot}$, where the former is the horizontal force leading to collapse and applied at the top left corner of the frame, and the latter is the total weight of the masonry frame (Figure 7): $W_{tot} = W_1 + W_2 + W_3 + W_4 + W_5$, where $W_1$,...,$W_5$ refer to the weight of each of the blocks. The geometry of the frame and the considered forces are visible in Figure 7. The analytical formulae have been derived under the assumptions that cracks can only occur at the pier-to-spandrel connections (dashed lines in Figure 7), no tensile strength, infinite compression strength transferable across the cracks, and no sliding between blocks is allowed. Finally, the blocks are considered as rigid units and undergo only small displacements.

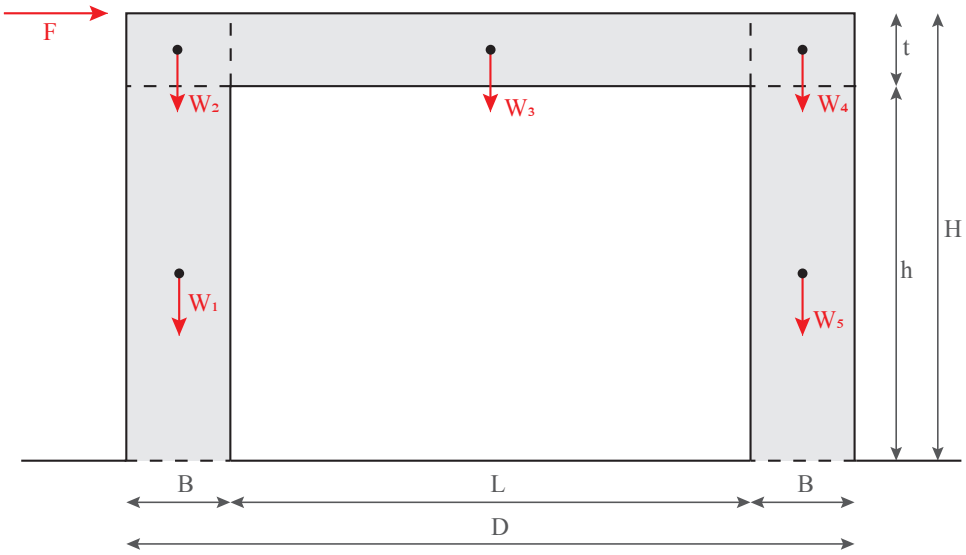


Figure 7: Geometry of the masonry frame with the applied forces. The possible crack lines are indicated with a dashed line.

Under these assumptions, the frame behaves as a rigid-block assembly of 5 macroblocks, and the collapse of the frame occurs by the formation of at least four hinges located on interfaces between rigid blocks. Since there are six interfaces, the total number of possible collapse mechanisms is 15. In [8], the analytical expression of the collapse load multiplier has been derived for only four of these 15 possible mechanisms, which are shown in Figure 8.

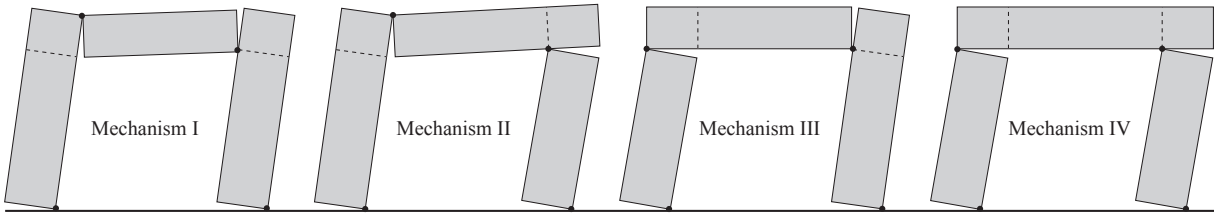


Figure 8: Collapse mechanisms considered in Giordano et al. [8].

The same frame has been implemented in the HybriDFEM code, with a height-to-width ratio $H/D$ equal to 1. The model is composed of seven blocks in total: the five macroblocks composing the frame, and one block under each pier representing the supports. These two base blocks are fixed in the three directions. The interface between each of the blocks is modeled as a no-tension interface, by assigning the following contact law to the contact faces:

$$\begin{cases} \sigma = 0 \quad \text{and} \quad \tau = 0 & \text{when} \quad \varepsilon > 0 \\ \sigma = \varepsilon E_0 & \text{when} \quad \varepsilon \leq 0 \end{cases}, \tag{2}$$

in which $E_0$ is set to a very large value in order to approximate a rigid interface in compression. The self-weight of each macroblock is applied at its centroid, and the horizontal force $F$ is applied at the top left corner of the frame. This force is controlled by means of a displacement-control procedure on the horizontal displacement of the spandrel block. Considering that the collapse of the structure occurs when the program is not able to converge to an equilibrium solution, the collapse load multiplier $\alpha_{Num}$ of the frame is computed as the force $F$ applied at the last converged step divided by the total weight. Since this value of load multiplier corresponds to a structure on the brink of collapse, but still in equilibrium, it is expected to be slightly lower than the value of collapse load multiplier computed analytically.

Table 1 gives the collapse load multipliers obtained with the HybriDFEM model, and compares them with the ones obtained with kinematic analysis [8], for a ratio $B/D$ ranging from 0.1 to 0.4 and a ratio $t/H$ ranging from 0.1 to 0.3. The percentage error between both values, which corresponds to the difference between the numerical and analytical value, divided by the analytical one, is also provided. The load multipliers obtained with the HybriDFEM compare well with the analytical ones, with a maximal error of -2.45%. As expected and discussed, the numerical load multiplier is always slightly smaller than the analytical one. All simulations with $B/D = 0.4$ triggered the collapse mechanism III (Figure 9a), which corresponds to what was predicted analytically [8]. However, while the expected collapse mechanism for all other values of $B/D$ was mechanism I, the HybriDFEM model triggered a fifth collapse mechanism (Figure 9b) that was not taken into account in the original paper. These frames were run again with only three macroblocks in order to force mechanism I, and the associated value of $\alpha_{num}$ was always slightly higher than the one triggering mechanism V, but still lower than the analytical collapse load multiplier associated to mechanism I. This tends to indicate that the choice to consider only four mechanisms out of the 15 possible was not always conservative, even if the load multiplier associated to the fifth mechanism was never less than 2% lower than the one associated with Mechanism I.

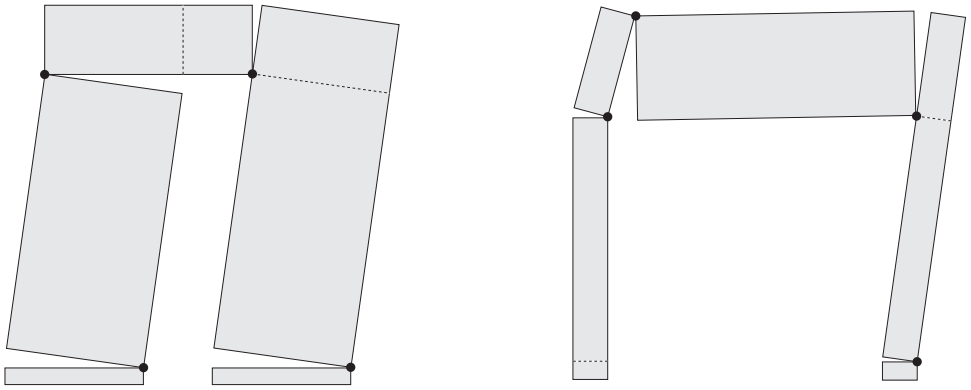

(a) (b)

Figure 9: (a) Mechanism III triggered for $t/H = 0.2$ and $B/D = 0.4$ and (b) Mechanism V triggered for $t/H = 0.3$ and $B/D = 0.1$ with the HybriDFEM.

| $t/H$ $\downarrow$ | $B/D$ $\rightarrow$ | 0.1 | 0.2 | 0.3 | 0.4 |
|---|---|---|---|---|---|
| 0.1 | $\alpha_{LA}$ | 0.054 | 0.109 | 0.165 | 0.238 |
| | $\alpha_{Num}$ | 0.053 | 0.107 | 0.167 | 0.235 |
| | Err. [%] | -1.98 | -1.56 | -1.20 | -1.26 |
| 0.2 | $\alpha_{LA}$ | 0.06 | 0.122 | 0.195 | 0.286 |
| | $\alpha_{Num}$ | 0.059 | 0.121 | 0.193 | 0.282 |
| | Err. [%] | -2.45 | -1.13 | -1.09 | -1.40 |
| 0.3 | $\alpha_{LA}$ | 0.07 | 0.144 | 0.247 | 0.346 |
| | $\alpha_{Num}$ | 0.069 | 0.142 | 0.245 | 0.342 |
| | Err. [%] | -0.98 | -1.10 | -1.10 | -1.15 |

Table 1: Collapse load multipliers obtained analytically from [8] ($\alpha_{LA}$) and numerically with the HybriDFEM ($\alpha_{Num}$).

## 5 CONCLUSIONS

The HybriDFEM method presented in this paper as an extension of the Fibre Contact Element Method (FCEM) [7], models a structure as an assembly of rigid blocks. This method shares similitudes with the Applied Element Method (AEM) in that the deformation is concentrated at the block interfaces, which are modeled as distributed nonlinear springs. But it also differs from it in the measure that it can include springs connected in series at the interfaces, allowing to differentiate, for instance, the relative deformations of two blocks made of a different material. The HybriDFEM, which is discontinuous by nature, can be used as a proxy to model continuous structures through the use of scaled spring constitutive models [2]. Here it was shown that several members can be connected through rigid-node connections in order to model discontinuous frames.

After a brief overview of the theoretical developments of the method, two benchmark problems have been implemented and compared with classical FEM or analytical solutions. The first benchmark, which consisted of a frame made of a continuous material, highlighted the capacity

of the method to capture nonlinear geometric effects (here $P - \Delta$ effects) and to use nonlinear material models (here an elastic-perfectly plastic material). It was shown that the HybriDFEM could be coupled with a classical Timoshenko beam element accounting for nonlinear geometric effects. The second benchmark consisted of a masonry portal frame in which the crack lines were pre-defined at the pier-to-spandrel connections. The frame has been modeled as an assembly of five rigid blocks assembled through rigid no-tension interfaces. The horizontal capacity of the masonry frame with different geometries has been computed with the HybriDFEM and compared with analytical values from the literature. The results showed a maximum relative error of -2.45% between the HybriDFEM and the analytical values, and expanded the number of possible collapse mechanisms to include those that were not considered in [8].

Ongoing developments of the HybriDFEM include the extension to dynamic problems, the modeling of reinforced concrete (RC) beams and the extension to two-directionally spread members. The formulation is developed with the intention to resemble that of a classical FEM, allowing hybrid simulations to be carried out with small computational demand, while simultaneously and explicitly modelling discontinuities.

## 6 Acknowledgements

The first author is thankful for the financial support given by UCLouvain.

## REFERENCES

[1] D. Baraldi, E. Reccia, and A. Cecchi. In plane loaded masonry walls: Dem and fem/dem models. a critical review. *Meccanica*, 53(7):1613–1628, 2017.

[2] I. Bouckaert, M. Godio, and J. Almeida. A hybrid discrete-finite element method for modeling continuous and discontinuous beam-like members including nonlinear geometric and material effects. *Under review*, 2023.

[3] S. Casolo and G. Uva. Nonlinear analysis of out-of-plane masonry façades: full dynamic versus pushover methods by rigid body and spring model. *Earthquake Engineering Structural Dynamics*, 42(4):499–521, 2013.

[4] P. A. Cundall. A computer model for simulating progressive large scale movements in blocky rock systems. In *Symposium of the International Society for Rock Mechanics*, volume II-8. Society for Rock Mechanics (ISRM).

[5] R. de Borst, M. A. Crisfield, J. J. C. Remmers, and C. V. Verhausel. *Non-Linear Finite Element Analysis of Solids and Structures*. Wiley Series in Computational Mechanics. Chichester, 2 edition, 2012.

[6] J. M. C. Estêvão and A. S. Carreira. Using the new fibre contact element method for dynamic structural analysis. *Engineering Structures and Technologies*, 7(1):24–38, 2015.

[7] J. M. C. Estêvão and C. S. Oliveira. A new analysis method for structural failure evaluation. *Engineering Failure Analysis*, 56:573–584, 2015.

[8] A. Giordano, A. De Luca, E. Mele, and A. Romano. A simple formula for predicting the horizontal capacity of masonry portal frames. *Engineering Structures*, 29(9):2109–2123, 2007.

[9] J. Lemos. Discrete element modeling of the seismic behavior of masonry construction. *Buildings*, 9(2):43, 2019.

[10] K. Meguro and H. Tagel-Din. Simulation of buckling and post-buckling behavior of structures using applied element method. *Bull. ERS*, 32, 1999.

[11] A. Munjiza and J. P. Latham. Computational challenge of large scale discontinua analysis. *Third International Conference on Discrete Element Methods*, 2002.

[12] F. P. A. Portioli. Rigid block modelling of historic masonry structures using mathematical programming: a unified formulation for non-linear time history, static pushover and limit equilibrium analysis. *Bulletin of Earthquake Engineering*, 18(1):211–239, 2020.

[13] P. Roca, M. Cervera, G. Gariup, and L. Pela'. Structural analysis of masonry historical constructions. classical and advanced approaches. *Archives of Computational Methods in Engineering*, 17(3):299–325, 2010.

[14] W. Rust. *Non-Linear Finite Element Analysis in Structural Mechanics*. 2015.

[15] H. Tagel-Din and K. Meguro. Applied element simulation for collapse analysis of structures. *Bull. ERS*, 32, 1999.